ACS Catalysis

Research Article

pubs.acs.org/acscatalysis

Effects of Drying Conditions on the Synthesis of Co/SiO_2 and Co/Al_2O_3 Fischer–Tropsch Catalysts

Peter Munnik, Nynke A. Krans, Petra E. de Jongh, and Krijn P. de Jong*

Inorganic Chemistry and Catalysis, Debye Institute for Nanomaterials Science, Utrecht University, Universiteitsweg 99, 3584 CG Utrecht, The Netherlands

Supporting Information

ABSTRACT: The nanoscale distribution of the supported metal phase is an important property for highly active, selective, and stable catalysts. Here, the nanoscale redistribution and aggregate formation of cobalt nitrate during the synthesis of supported cobalt catalysts were studied. Drying over a range of temperatures in stagnant air resulted in cobalt particles (8 nm) present in large aggregates (30–150 nm). However, drying in a N_2 flow resulted in cobalt nanoparticles distributed either in aggregates or uniformly on various SiO_2 and γ-Al_2O_3 supports, critically dependent on the drying temperature. The mechanism of aggregation was studied through chemical immobilization of the precursor on a silica support after drying in a N_2 flow. The aggregation behavior upon drying in a gas flow at temperatures below 100 °C showed a remarkable similarity to distributions obtained upon the dewetting of colloidal films, suggesting a physical process. Alternatively, by inducing decomposition of the cobalt nitrate above 100 °C before drying was complete, aggregation was brought about through a chemical process that occurred both in stagnant and flowing gas. A γ-alumina support exhibited increased precursor-support interactions and displayed little cobalt aggregation upon drying in a gas flow but extensive aggregation upon drying in stagnant air. The aggregation behavior was further tested on silica supports with pore sizes between 3 and 15 nm and tested under industrially relevant Fischer–Tropsch conditions, which revealed that uniform cobalt nanoparticle distributions were up to 50% more active compared to aggregated systems. Thus, hydrodynamics and the temperature of the gas phase are critical parameters to control nanoscale distributions during drying of functional nanomaterials such as supported catalysts.

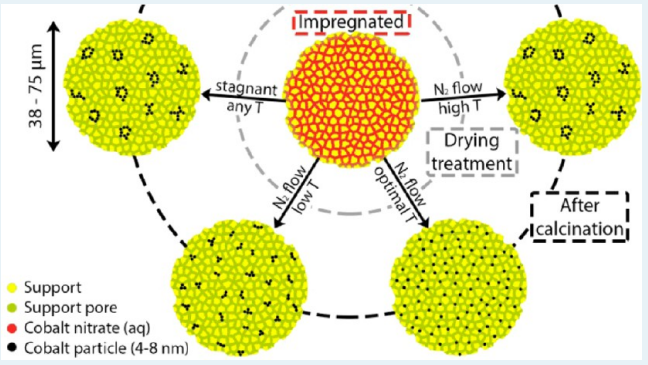

KEYWORDS: *cobalt, Fischer–Tropsch, drying, impregnation, catalyst preparation, distribution, immobilization*

INTRODUCTION

Supported transition metal nanoparticles are used as catalysts in many industrial processes. The size, composition, and chemical environment of these particles as well as their distribution over the support greatly influences the activity, selectivity, and stability of the catalysts.[1−4] Therefore, control over the synthesis of these nanomaterials is of the utmost importance.[5−7] However, although the number of fundamental studies on catalyst preparation is increasing, the physiochemical processes that take place during synthesis are often not understood.

A facile and cost-effective preparation method is the impregnation of a metal precursor solution onto a porous support, such as alumina, silica, or titania. The impregnation can be done to incipient wetness, whereby the impregnating volume is equal to the pore volume of the support, eliminating the need for a filtration step. Evaporation of the solvent, followed by decomposition of the precursor via a thermal treatment, leads to supported metal oxides. Metal nitrates precursors are often used, as their high solubility allows for high metal loadings in a single impregnation step. However, poor metal oxide dispersions and inhomogeneous distributions of the metal oxide are frequently obtained. Many studies report on improvement by changing the solvent or precursor,[8−15] coimpregnation with organic molecules,[7,16−19] or modifying the drying or calcination procedure.[20−28] However, fundamental knowledge on, and control over, inhomogeneous metal oxide distributions and precursor redistribution is lacking.

The drying step has long been known to have a large impact on the macroscopic distribution of the active phase, especially for impregnations with diluted precursor solutions.[29,30] Recently, models have shown that at high nickel nitrate concentrations, homogeneous macroscopic distributions can be obtained after impregnation and drying.[31] More recently, using freeze-drying it was shown that the drying step can also have a large influence on the nanometer scale distribution of cobalt nitrate on silica gel supports.[32,33] The nanoscale redistribution was further controlled by drying in a N_2 fluidized bed reactor at

Received: May 19, 2014
Revised: July 21, 2014
Published: August 5, 2014

   dx.doi.org/10.1021/cs5006772 | ACS Catal. 2014, 4, 3219–3226

different temperatures.[34] Both low and high drying temperatures resulted in the formation of agglomerates, and an optimum temperature of 100 °C was found whereby homogeneous distributions were obtained.

When silica is used as a support, the low point of zero charge (PZC), generally between a pH of 3 and 4, results in little electrostatic interaction between the support and cobalt ions of the metal nitrate precursor solution, which has a similar pH. In contrast, electrostatic interactions[5,35] could start to play a role in the drying and agglomeration process on γ-alumina, also a widely used support in academia and industry but which has a higher PZC of 8−9. Alternatively, metal nitrates can be immobilized through the use of nitric oxide (NO), which stimulates the hydrolysis of several metal nitrates at low temperatures, leading to the formation of metal hydroxynitrate phases $(M_x(OH)_y(NO_3)_z$, whereby M = Cu, Ni, or Co).[23,28,36,37] This phase is immobile, and further heat treatment leads to oxygen scavenging by NO during the decomposition of cobalt (hydroxy)nitrate and the formation of small cobalt oxide particles.[20,23,38]

In this contribution, we further study the mechanism and compounds involved in the nanoscale redistribution of cobalt nitrate during drying. We first show that the formation of cobalt hydroxynitrate is possible for an impregnated and dried $Co(NO_3)_2/SiO_2$ sample with low water content. This precursor immobilization technique was subsequently used to study the drying imprint on the nanoscale distribution of cobalt on silica gel at different temperatures. Next, a γ-alumina support was studied, and finally the effect of pore size on the nanoscale distribution was studied using different silica gels, as well as the impact of the cobalt nanoscale distribution on the activity and selectivity in the Fischer−Tropsch synthesis.

EXPERIMENTAL SECTION

Sample Preparation. Commercially available silica gels (SG) and γ-alumina (GA) were used as supports (Table 1. Davicat, Grace-Davidson and Puralox, Sasol). Before precursor loading, the support was sieved to a grain size of 38−75 μm. Solution impregnation was performed to incipient wetness using a saturated $Co(NO_3)_2$ (aq) solution (4.2 M, $Co(NO_3)_2 \cdot 6H_2O$, >99% Sigma-Aldrich) at room temperature under a static vacuum.

Table 1. Physical Properties of the Supports and Final Cobalt Loading for the Corresponding Catalysts

support[a]	BET surface area (m^2/g)	pore volume (P/P_o = 0.93) (mL/g)	average pore diameter (nm)	Co loading (wt %)
SG3	720	0.5	3	10
SG8	500	0.9	8	16
SG15	330	1.2	15	21
GA9	250	0.5	9	17

[a]SG = silica gel, GA = γ-alumina; number refers to the average pore size (nm).

Different drying treatments were applied to 100−400 mg of the impregnated grains in a fluidized bed reactor. The oven was first brought to a temperature of 25, 50, 75, 100, 125, or 150 °C, after which the sample was introduced and a N_2 flow was applied with a gas hourly space velocity (GHSV) of 5000 h^{-1} for 48, 24, 16, 3, 3, or 2 h, respectively. As reported previously, these drying times were sufficient to induce precipitation of the precursor, while greatly extended drying times did not alter the nanoscale distributions of the final catalysts.[34] Alternatively, the sample was cooled to −45 °C for 5 h under N_2, and drying was performed at −30 °C at reduced pressure (0.02−0.03 mbar) for 3 days,[32] or drying was performed at room temperature in a dynamic vacuum (∼50 mbar) or in a muffle oven at 90 °C for 1 day or 8 h, respectively. Calcination of all dried catalysts was performed by transfer to or further heating of the fluidized bed reactor to 350 °C (1 °C/min, 1 h) in a flow of pure N_2 or 1% v/v NO/N_2 (GHSV 30000 h^{-1}). In this study, NO was used to immobilize the precursor after drying by formation of cobalt hydroxynitrate. However, this also led to very small particles, which can be difficult to image and are undesirable for the Fischer−Tropsch synthesis. Because calcination in a N_2 flow results in somewhat larger particles, it was used for the γ-alumina samples and the samples that were used for catalysis. For γ-alumina, after calcination the sample was impregnated, dried, and calcined a second time to increase the metal loading.

Characterization. N_2-physisorption measurements were performed at −196 °C using a Micromeritics Tristar 3000 apparatus. Prior to analysis, samples were dried in a He flow for 16 h at 200 °C. Average pore diameter was calculated using the BJH desorption isotherm.

Thermogravimetric analysis (TGA, Q50 TA Instruments) was used to determine the residual water content of impregnated samples after different drying treatments by measuring the weight loss after heating to 500 °C for 30 min (10 °C/min) under a 60 mL/min N_2 flow. The weight loss was corrected for the loss of water by desorption and condensation of silanol groups from the pristine silica gel, which was experimentally found to occur between 150 and 500 °C. The rest of the weight loss was attributed to the loss of any residual water and the decomposition of $Co(NO_3)_2$ to Co_3O_4.

TGA-MS was measured on a Pyris 1 TGA, (PerkinElmer). About 10 mg of the impregnated silica was heated at 5 °C/min to 800 °C. Above 300 °C, no significant weight loss or MS signals were detected.

In situ diffuse reflectance infrared Fourier transform spectroscopy (DRIFTS) measurements were performed on a Bruker Tensor 27 apparatus utilizing a HVC-DRP-3 diffuse reflectance reaction chamber with CaF_2 windows and a high-sensitivity liquid N_2-cooled MCT detector. To minimize temperature gradients, the bottom of the bed was filled with SiC, which was separated from the sample by a grid. One-percent v/v NO in N_2 or pure N_2 was flown through 10 mg of sample at 10 mL/min from top to bottom while the chamber was heated to 300 °C at 2 °C/min. Spectra were taken at a resolution of 4 cm^{-1} at 2 min intervals.

X-ray diffraction (XRD) patterns were recorded between 20 and 90° 2θ with a Bruker-AXS D2 Phaser X-ray Diffractometer using Co $K_{\alpha 12}$ radiation (λ = 1.790 Å). The volume averaged Co_3O_4 crystallite size was determined using the Scherrer equation with a shape factor k = 0.9 and line broadening analysis on the (220), (311), and (400) peaks by a fitting procedure in the Eva2 software (Bruker AXS).

The catalyst grains were embedded in a two component epoxy resin (Epofix, EMS) and cured at 60 °C overnight. The embedded catalysts were then cut into thin sections with a nominal thickness of 50 nm using a Diatome Ultra 35° diamond knife mounted on a Reichert-Jung Ultracut E microtome and collected on a copper grid. Bright field transmission electron microscopy (TEM) images were obtained on a Tecnai 12, operated at 120 keV. High angle

dx.doi.org/10.1021/cs5006772 | ACS Catal. 2014, 4, 3219−3226

annular dark field (HAAFD) STEM was performed on a Tecnai 20 equipped with a field emission gun operated at 200 keV.

Catalytic Testing. Fischer–Tropsch synthesis was performed on a Flowrence (Avantium) 16 parallel reactor unit. Each stainless steel reactor was loaded with the same amount of cobalt, resulting in a weight loading of 80, 50, or 40 mg for catalysts made from SG3, SG8, or SG15, respectively. Catalysts were mixed with 200 mg of SiC and reduced in situ in 25 vol % H_2/He at 500 °C for 8 h (1 °C/min). Afterward, the reactors were cooled down to 180 °C at which the pressure was increased to 20 bar under H_2. Next, the feed was changed to a H_2/CO ratio of 2.0 with 5 vol % He, which functioned as an internal standard for the online GC (Agilent 7890A). After 1 h, the temperature was increased to the reaction temperature of 220 °C at 1 °C/min. After 100 h on-stream, the conversion was lowered by increasing the gas hourly space velocity (GHSV) so that the performance of all catalysts could be reported at 30–35% conversion, eliminating effects of conversion on selectivity.

RESULTS AND DISCUSSION

Hydroxynitrate Formation. To study the cobalt nitrate distributions on a silica gel with 8 nm pores (SG8) after different drying treatments, samples were subjected to a thermal treatment in 1% v/v NO/N_2 after drying. This treatment is known to induce the formation of cobalt hydroxynitrate,[23,28,36,37] an immobile phase that prevents further redistribution upon thermal decomposition into cobalt oxide. NO-assisted decomposition of cobalt nitrate also results in smaller particles compared to decomposition in stagnant air or a N_2 flow.[20] To ensure hydrolysis of cobalt nitrate did occur after drying, an *in situ* Diffuse Reflectance Infrared Fourier Transform Spectroscopy (DRIFTS) study was performed in 1% v/v NO/N_2 on a cobalt nitrate loaded SG8 sample impregnated and dried at 100 °C in N_2. Figure 1 shows the

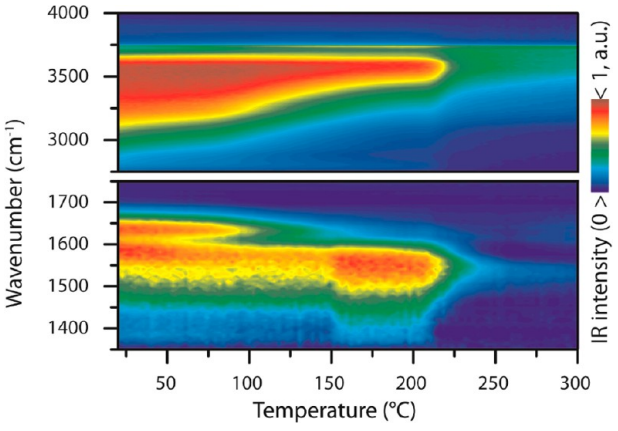

Figure 1. *In situ* DRIFTS of cobalt nitrate loaded SG8 during calcination in 1% NO after impregnation and drying at 100 °C in N_2. Formation of an OH^- peak at 3585 cm^{-1} combined with an NO_3^- peak at 1540 cm^{-1} is characteristic of the formation of cobalt hydroxynitrate. Above 200 °C, the peaks disappear in a single step, indicating direct decomposition to Co_3O_4.

spectrum evolution during heat treatment. The initial broad –OH stretching vibration band between 3100 and 3600 cm^{-1} accompanied by a sharp H–O–H bending vibration band at 1630 cm^{-1} indicated some water was still present after drying. These bands gradually decreased, and at 150 °C a sharp –OH band formed at 3585 cm^{-1}, accompanied by a shift in the –O–N–O_2 stretching vibration band from the nitrate group from 1580 to 1540 cm^{-1}. These bands were previously attributed to cobalt hydroxynitrate species[23,36] and disappeared simultaneously above 200 °C, when Co_3O_4 was formed.

The mass loss upon heating was investigated by Thermogravimetric Analysis (TGA). The SG8 sample after impregnation and drying at 100 °C in N_2 showed a remaining water content of about 0.4 $mol_{H_2O}/mol_{Co(NO_3)_2}$. This suggests that a phase with an OH/Co ratio of at most 0.5 was formed ($Co_2OH(NO_3)_3$), whereas previous studies reported hydroxynitrates with higher hydroxyl content ($Co_3(OH)_4(NO_3)_2$ or $Co_2(OH)_3NO_3$).[23,28] However, TGA results might underestimate the remaining water content, and it is possible that surface hydroxyl groups of the silica or strongly adsorbed water contributed to the formation. Moreover, the formation of cobalt hydroxynitrate need not be quantitative. Regardless, it was clear that even after drying, hydroxynitrates were formed via the NO assisted hydrolysis of cobalt nitrate.

Precursor Immobilization. The nanoscale distributions of six SG8 supported Co_3O_4 catalysts calcined in 1% NO at 350 °C with a ramp of 1 °C/min are shown in Figure 2. The drying temperature before calcination was varied between 25 and 150 °C. The sample dried at 25 °C exhibited cobalt as small 3 to 4 nm particles in large irregular aggregates. These nanoparticle aggregates were 100 to 200 nm long and 50 to 100 nm wide, many times the average support pore size of 8 nm. Increasing the drying temperature resulted in gradually smaller aggregates until at 100 °C a homogeneous distribution of similarly sized 3 to 4 nm cobalt crystallites was observed. Drying at 125 °C resulted in a bimodal distribution of the small homogeneously distributed particles and aggregates of 15–20 nm, consisting of 8 nm particles. After drying at 150 °C, most of the cobalt was located as 8 nm particles in 50 nm spherical aggregates, whereas few small particles were found.

These results illustrate the two possible ways of aggregate formation previously postulated.[34] At temperatures between 25 and 100 °C, a difference in the drying rate resulted in a different degree of aggregation during the precipitation of cobalt nitrate species. This aggregation occurred in the form of irregular domains as large as 200 nm, more than 20 times the size of the average pore. During the subsequent heat treatment in 1% NO, this precipitated phase was converted into cobalt hydroxynitrate, which decomposed into small cobalt oxide nanoparticles at higher temperatures. Since one immobile phase was converted into another, little redistribution occurred, so that the resulting patterns are the imprint of where the cobalt nitrate precipitated during drying.

At drying temperatures above 100 °C, part of the cobalt nitrate started to decompose into Co_3O_4 during the drying process. Previously, it was shown that 20% of the cobalt nitrate decomposed into Co_3O_4 during drying at 125 °C.[34] This decomposition occurred in the absence of NO, but in the presence of H_2O, which induces mobility and leads to larger particles and aggregation,[20,23,39] forming small (15–20) nm aggregates of 8 nm particles. The remaining 80% of the cobalt nitrate which did not decompose during drying was subsequently exposed to NO during further heat treatment, which resulted in small (3–4) nm nanoparticles, explaining the bimodal distribution. At a drying temperature of 150 °C, more cobalt nitrate decomposed during drying, resulting in many 8 nm particles located in 50 nm spherical aggregates that formed during drying, while little unreacted cobalt nitrate remained to

dx.doi.org/10.1021/cs5006772 | ACS Catal. 2014, 4, 3219–3226

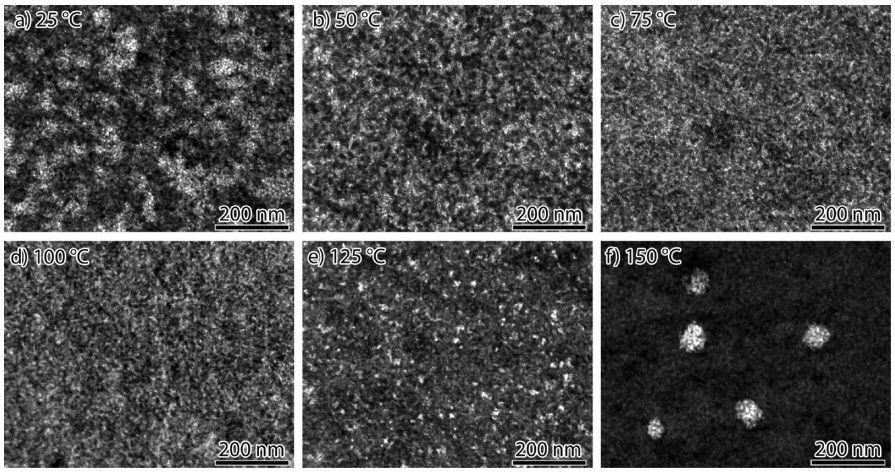

Figure 2. HAADF-STEM images of SG8 supported Co_3O_4 catalysts after calcination in 1% NO at 350 °C, whereby the drying temperature in a N_2 flow (before calcination) was varied between 25 and 150 °C. Different aggregates of cobalt nanoparticles (white) were found on the silica SG8 support (black) depending on the drying temperature. (a) Dried at 25 °C, (b) 50 °C, (c) 75 °C, (d) 100 °C, (e) 125 °C, (f) 150 °C.

form 3−4 nm cobalt particles via NO-assisted decomposition. Although drying can affect the macroscopic distribution across pellets or grains, homogeneous distributions were observed on these larger length scales.

Similar patterns to those observed after drying between 25 and 100 °C have been found in different fields of physics and chemistry, most noticeably in the drying of colloidal wet films.[40−44] The drying of colloidal systems has been extensively studied, and models have been proposed that explain the patterns found experimentally for a wide variety of colloids, solvents and substrates. In those models, the drying temperature, and so the drying rate, was found to be key in obtaining differently sized aggregates and patterns. At a high drying rate, solvent evaporation is thought to occur throughout the entire film within a very short time window, called spinodal dewetting, resulting in deposition of the colloids close to where they were in solution. At lower rates, dewetting does not occur homogeneously or as rapidly, so that colloids can move and gather in patches, which increase in size with decreasing temperature. Despite the fact that a colloidal dispersion on a flat surface is very different from a dissolved salt in a 3D porous network, such as in the present work, the similar temperature dependency is remarkable. (For an example, compare the results obtained here after drying at 25 and 50 °C with the third and fourth column of Figure 1 in ref 43.) It appears that in both cases, redistribution of the liquid phase, which is determined by the rate of drying, determines the final distribution of particles.

At very low drying rates, the colloidal dewetting models predict the formation of large cellular networks, whereby the cell walls are made up of colloids whereas the cell bodies are empty. Very slow drying is thought to lead to isolated gas bubbles that nucleate and subsequently grow, entraining the colloidal rich phase along in the meniscus surrounding the growing gas bubble. Deposition of colloids occurs when two menisci meet, at which point all the material is deposited in the thin strands forming the cell walls, enclosing mostly empty cells where the gas bubble used to be. A similar mechanism could be envisioned in porous media, whereby growing gas bubbles inside the impregnated support[45] forces the dissolved precursor into increasingly concentrated areas, until the menisci of two bubbles meet and the salt concentration suddenly exceeds the supersaturation, causing precipitation. To investigate this, cobalt nitrate impregnated on silica gel (SG8) was dried at −30 °C under reduced pressure, followed by calcination in 1% NO. It should be noted that this drying temperature was previously found to be insufficient to freeze the precursor, such that redistribution was possible.[32] The resulting material exhibited a cellular network whereby the cells were made up of empty silica, while the cell walls were cobalt rich and connected to other cells (Figure 3a). It is remarkable that a relatively simple 2D model of colloidal particles in a liquid film behaves very similar to a complicated 3D system in which a salt precursor precipitates from a solution.

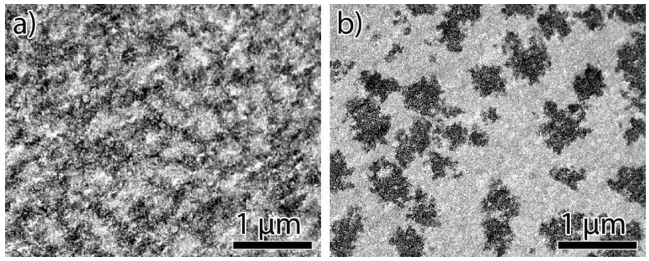

Figure 3. Bright field TEM images of two Co_3O_4 (in black) catalysts on SG8 created by heat treatment in a 1% NO atmosphere. (a) Dried at −30 °C in a vacuum, whereby a cellular network was formed, followed by calcination in NO. (b) Directly calcined in an NO/N_2 flow without prior drying in a N_2 flow, resulting in large nanoparticle islands.

An alternative explanation may be found in capillary flow phenomena. Capillary flow can lead to inhomogeneous distributions, especially in supports with bi- or multimodal pore size distributions, whereby the meniscus at the drying front recedes from larger to smaller pores, entraining the dissolved precursor with it.[29] Figure S4 shows the pore size distributions of all support materials, which were relatively narrow and monomodal. Nonetheless, for drying at low temperatures such as at 25 °C, capillary flow may be significantly faster than the drying rate, so that capillary flow could play a role in the redistribution of the precursor phase. At higher temperatures, drying may be faster relative to capillary flow, especially if highly viscous cobalt nitrate tetra- or dihydrates form, so that redistribution may be limited.

dx.doi.org/10.1021/cs5006772 | ACS Catal. 2014, 4, 3219−3226

Regardless of the mechanism, it is clear that aggregate formation at 100 °C can be limited by applying a N_2 flow leading to a fast drying rate based on physical processes.

Drying at higher temperatures showed that aggregation can also occur via a chemical process, through nucleation and growth of cobalt oxide from a cobalt nitrate solution. To explore whether a similar effect could be created at lower temperatures, a sample was directly dried and heat treated in a 1% NO/N_2 flow after impregnation, without a drying step in a N_2 flow. Figure 3b shows this led to the formation of large islands of a few hundred nanometers, separated by large empty areas. This behavior is understood by the nucleation and growth of a hydroxynitrate phase from a liquid precursor. As soon as nucleation of the precipitate occurs, further growth resulted in large cobalt hydroxynitrate patches, which are subsequently converted to small cobalt oxide particles at higher temperatures. These patches could even become several micrometers in size (see Supporting Information, Figure S1). Thus, although aggregate formation can occur through a physical process, whereby it is mainly dependent on the drying rate, the chemistry of the system remains highly relevant and can dominate aggregate formation.

γ-Alumina Support. Compared to silica, which has a PZC of 3−4, γ-alumina shows a stronger interaction with the precursor solution of pH 3 because of its high PZC (8−9). This could affect the impregnation and drying step, and adsorption of Co^{2+} complexes onto the support via a ligand exchange between water and surface hydroxyl groups has been observed.[46−48] To investigate whether such support precursor interactions influence the aggregation behavior of cobalt nitrate, a γ-alumina with 9 nm pores (GA9) was impregnated and dried at different temperatures. Again, heat treatment in 1% NO/N_2 after drying resulted in very small particles, as is known from the literature.[37,49] However, these particles were very difficult to image, even after a double impregnation to increase the loading from 9 to 17 wt % (see Supporting Information, Figure S2). For this reason, the heat treatment after drying was performed in N_2 rather than NO. In a N_2 flow, hydroxynitrates do not form despite the high pH of the support, so that larger particles were obtained that allowed clear visualization of the spatial distribution.

On γ-alumina, aggregate formation is often reported in the context of Fischer−Tropsch catalysts.[50,51] Attempts to avoid the formation of aggregates include modification of the support[52] or coimpregnation with organic molecules.[16] However, these strategies only apply in specific cases. Conventional synthesis of such catalysts includes drying the impregnated material in stagnant air, often between 60 and 120 °C, before performing a calcination treatment. Figure 4a shows a sample dried at 90 °C in stagnant air followed by calcination in N_2. Cobalt particles of 8 nm were observed in irregularly shaped aggregates between 30−60 nm throughout the sample, similar to what is described in the literature. Drying at 60 and 120 °C showed comparable results, and drying at 150 °C resulted in even larger aggregates of 100−150 nm (see Supporting Information, Figure S3).

A large difference was observed upon drying in a N_2 fluidized bed. After drying at 25 and 100 °C, no aggregates were found at all (Figure 4b,c); the 7−8 nm sized particles were homogeneously distributed throughout the support. Even drying at 150 °C in a N_2 flow only resulted in small 20−30 nm aggregates (Figure 4d). Thus, although aggregates formed upon drying in stagnant air regardless of temperature on γ-alumina, a procedure whereby the sample was dried in a N_2 fluidized bed reactor completely prevented aggregation when a temperature between 25 and 100 °C was used, resulting in uniform nanoparticle distributions.

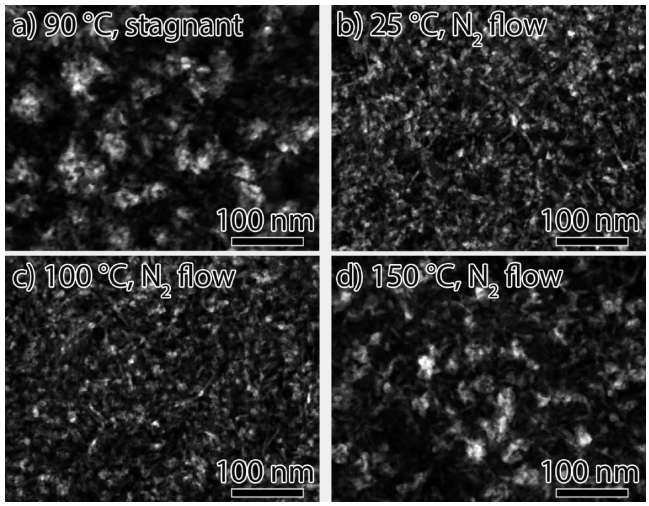

Figure 4. HAADF-STEM images of Co_3O_4 (white) on γ-alumina (GA9) using different drying treatments, followed by calcination at 350 °C in a N_2 flow. (a) Dried at 90 °C without a gas flow. (b) Dried in a N_2 fluidized bed at 25 °C, (c) 100 °C, and (d) 150 °C.

Upon comparing γ-alumina with silica, discussed in the previous section, the homogeneous distribution observed on γ-alumina after drying at 25 °C is remarkable and suggests the increased precursor-support interactions suppressed the formation of aggregates at low temperatures. Although N_2 was used during heat treatment, so that some redistribution might be expected, previous results on SiO_2 heat treated in N_2 showed aggregates were also present at low temperatures on SiO_2,[34] so that the difference cannot be explained by the alternative heat treatment. Even at 150 °C, aggregates were smaller than those found on SiO_2. However, removing the gas flow during drying greatly increased the size of the aggregates (see Supporting Information), underlining the importance of a gas flow regardless of the temperature.

Influence of Pore Size. To further investigate aggregate formation, three different silica supports with pore sizes of 3, 8, and 15 nm were impregnated and dried in a N_2 flow at 25, 100, and 150 °C. To study the effect of drying on Fischer−Tropsch catalysis, subsequent calcination was performed in N_2 rather than NO to form larger 7−11 nm sized particles, which are more favorable for the Fischer−Tropsch synthesis.[53−55] Figure 5 shows the nanoscale cobalt distribution of silica with 3 nm pores (SG3, top row), 8 nm pores (SG8, middle row), and 15 nm pores (SG15, bottom row). For each silica, drying at 25 °C led to the formation of medium sized aggregates (left column), drying at 100 °C resulted in homogeneous distributions (middle column), while after drying at 150 °C (right column) large aggregates were observed. The average sizes of the aggregates and average Co_3O_4 crystallite sizes as determined by TEM and XRD, respectively, are shown in Table 2. For the catalysts dried at 25 °C, a trend toward smaller aggregate sizes for larger pore sizes was observed, while this trend is less evident after drying at 150 °C. The Co_3O_4 crystallite sizes ranged from 8 to 12 nm regardless of pore size, even for SG3. While this could indicate extensive deposition of cobalt on the external surface, this was not observed. Thus, it appeared cobalt

dx.doi.org/10.1021/cs5006772 | ACS Catal. 2014, 4, 3219−3226

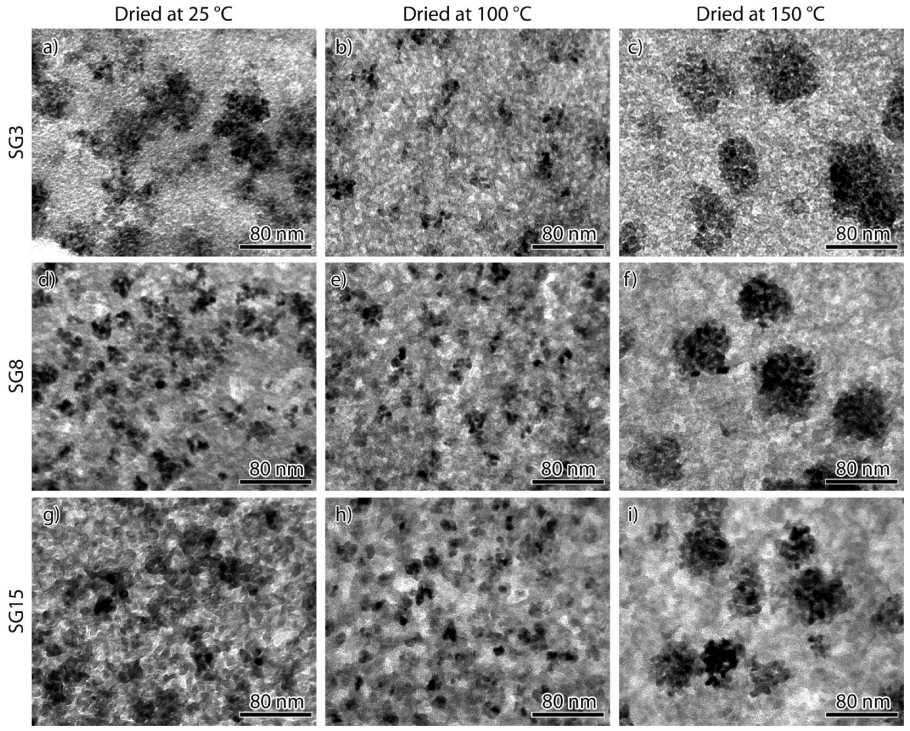

Figure 5. TEM of *ex-nitrate* cobalt catalysts synthesized using three different silica gels and three different drying temperatures, followed by calcination in N_2. (Top row) Silica gel with 3 nm pores. (Middle row) Silica gel with 8 nm pores. (Bottom row) Silica gel with 15 nm pores. (Left column) Dried at 25 °C. (Middle column) Dried at 100 °C. (Right column) Dried at 150 °C.

Table 2. Catalyst Properties after Calcination and Catalytic Results during Fischer−Tropsch Synthesis, Measured after 100 h on Stream at 20 bar, H_2/CO ratio of 2.0, 220 °C, 30−35% CO Conversion

silica pore size (nm)	drying temperature (°C)	crystallite size (XRD) (nm)	aggregate size (TEM) (nm)	CTY (10^{-5} $mol_{CO}·g_{Co}^{-1}·s^{-1}$)	C_1 (wt %)	C_{5+} (wt %)
SG3	25	8	50	4.3	13.1	75.5
	100	8	–	4.6	13.8	74.9
	150	7	65	4.7	13.1	75.9
SG8	25	8	20	5.2	10.0	81.5
	100	8	–	5.6	10.1	81.5
	150	9	60	5.0	8.9	83.3
SG15	25	10	16	7.2	9.1	84.1
	100	10	–	7.7	10.9	81.6
	150	11	55	5.2	8.6	85.2

was either preferentially deposited in larger pores or the growth of Co_3O_4 crystallites deformed or locally broke up the silica structure.

The decrease in aggregate size for larger pore silicas obtained after drying at 25 °C indicated that also the support pore structure played an important role in the formation of aggregates when the drying rate was low. This is tentatively attributed to the increased drying rate that is possible for larger pore silicas,[45] thereby reducing the extent of redistribution. At 100 °C, this effect was less noticeable because a relatively fast drying rate was already achieved. Since drying at 150 °C concerned aggregate formation via decomposition, it was not affected significantly by the pore size. Finally, we note that a larger silica pore size (23 nm) exhibited macroscopic redistribution effects upon drying (Figures S5 and S6). This could be suppressed by using melt infiltration rather than solution impregnation (Figure S7), so that a reduced amount of solvent limited redistribution.

Catalysis. To investigate the influence of the interplay between pore size and spatial distribution on catalytic performance, the nine catalysts shown in Figure 5 were tested in the Fischer−Tropsch synthesis reaction, whereby hydrogen and carbon monoxide are converted into long chain hydrocarbons, at industrially relevant conditions (20 bar, H_2/CO ratio of 2.0, 220 °C). After 100 h, the gas flow was adapted such that for each catalyst the CO conversion was between 30 and 35%. The results are summarized in Table 2. Although the degree of aggregation is also known to affect the stability of the catalysts, this has been described in detail in a separate paper.[34] The cobalt-weight-based activities varied between 4.3 and 7.7 (10^{-5} $mol_{CO}·g_{Co}^{-1}·s^{-1}$), while the selectivity to long hydrocarbons chains with five carbons or more (C_{5+}) varied between 75 and 85 wt %. Comparison of the most homogeneous (obtained after drying at 100 °C) and the most aggregated (obtained at 150 °C) catalysts shows that in each case the uniform catalyst was most active, while the aggregated catalyst was most selective. Catalysts prepared by drying at 25 °C,

dx.doi.org/10.1021/cs5006772 | ACS Catal. 2014, 4, 3219−3226

which had intermediate aggregate sizes, generally lay in between these values. The catalysts based on SG3 showed the lowest activity and selectivity, averaging around 4.5 and 75.5 wt %, respectively, with little variation caused by the degree of aggregation. For SG8, medium activities and selectivities were found. The homogeneously distributed catalyst was 10% more active compared to the aggregated one, which in turn showed a 2% higher selectivity, similar to what was reported previously.[34] With SG15, the highest activities and selectivities and largest influence of the degree of aggregation were found. The homogeneously distributed catalyst was 50% more active than the aggregated one, which was 4% more selective.

It is clear that in general a larger pore size was favorable for the Fischer−Tropsch reaction, as has been studied and explained in detail before.[56−59] However, for the first time we show that the larger the pore size, the more important the role of the nanoscopic distribution in determining the activity and selectivity of the catalyst. Whereas the nanoscopic distribution in SG3 and SG8 only caused a maximum difference in activity of 10%, this difference could become as high as 50% in SG15. Although a comprehensive understanding of these effects would require more thorough investigation of the reduced catalysts, it is clear that the distribution of the metal oxide plays a large role in determining the final activity, selectivity, and stability.[34]

CONCLUSION

The mechanism of the nanoscale redistribution and aggregate formation of cobalt nitrate during the synthesis of supported cobalt catalysts was studied. On silica gel, heat treatment in a 1% NO gas flow was used after drying in a N_2 flow to immobilize cobalt nitrate via the formation of cobalt hydroxynitrates. Upon drying the impregnated sample in a nitrogen gas flow at 25 °C, small particles (3−4 nm) were located in large irregularly shaped aggregates (100−200 nm), many times the size of the pore diameter of the support (8 nm). Increasing the drying temperature in a gas flow reduced the size of the aggregates found after calcination in an NO-containing gas flow, until at 100 °C homogeneously distributed cobalt particles (3−4 nm) were found. This aggregation behavior greatly resembled the patterns observed in the literature for the dewetting of colloidal films. This similarity was extended toward very slow drying at −30 °C, resulting in the formation of a cellular network type distribution, whereby small particles (3−4 nm) made up the walls of large (200−500 nm) cells empty of cobalt. Moreover, although supports with relatively narrow support pore size distributions were used, capillary flow could play a role in the formation of aggregates. Regardless of the mechanism, these results strongly suggest that aggregate formation at these temperatures is the result of physical processes. Large cobalt aggregates (100−1000 nm) could also be formed by chemical processes at temperatures above 100 °C, which caused the deposition of Co_3O_4 from solution, or by hydroxynitrates precipitation during a heat treatment in a 1% NO flow without prior drying in N_2.

The role of the chemical nature of the support on the aggregation of cobalt nitrate was investigated using a γ-alumina, which exhibits stronger support−precursor interactions. Drying in stagnant air between 60 and 120 °C resulted in medium sized cobalt aggregates (30−60 nm) after calcination in N_2, similar to what is often found in the literature. However, drying at 25 and 100 °C in a N_2 flow resulted in homogeneous distributions, showing the importance of using a flow during drying and suggesting that increased precursor−support interactions suppressed the formation of aggregates. Even at 150 °C, only small aggregates (20−30 nm) were found upon drying in a N_2 flow, whereas drying in stagnant air at 150 °C resulted in large aggregates (100−150 nm), underlining the importance of drying in a N_2 flow regardless of the temperature.

The role of pore size on the aggregate formation upon drying in a N_2 flow was studied using silica gels with 3, 8, and 15 nm pores. Larger pores resulted in slightly smaller aggregates, possibly related to faster drying rates in larger pores. Testing these catalysts under industrially relevant Fischer−Tropsch conditions revealed that homogeneously distributed catalysts could be up to 50% more active compared to aggregated catalysts. Thus, the hydrodynamics of the gas phase and temperature during the drying process are critical for controlling the nanoscale distribution during the synthesis of nanomaterials and supported catalysts in particular.

ASSOCIATED CONTENT

Supporting Information

Additional TEM on Co_3O_4 on SG8 and GA9. Pore size distributions of all supports. TEM and SEM on Co_3O_4 on SG23 showing macroscopic redistribution of the cobalt phase, which was inhibited using melt infiltration. This material is available free of charge via the Internet at http://pubs.acs.org.

AUTHOR INFORMATION

Corresponding Author

*E-mail: k.p.dejong@uu.nl.

Notes

The authors declare no competing financial interest.

ACKNOWLEDGMENTS

The Netherlands Organization for Scientific Research is acknowledged for funding (NWO TOP 700.57.341). Mr. H. Meeldijk (Utrecht University) is acknowledged for HAADF-STEM measurements. Ms. M. Versluis-Helder (Utrecht University) is acknowledged for the TGA-MS measurements. Ms. E. van Donselaar (Utrecht University) is acknowledged for ultramicrotomy instructions. Mr. J. H. den Otter (Utrecht University) is acknowledged for N_2-physisorption measurements.

REFERENCES

(1) Farmer, J. A.; Campbell, C. T. *Science* **2010**, *329*, 933−936.
(2) Torres Galvis, H. M.; Bitter, J. H.; Khare, C. B.; Ruitenbeek, M.; Dugulan, A. I.; de Jong, K. P. *Science* **2012**, *335*, 835−838.
(3) Prieto, G.; Zečević, J.; Friedrich, H.; de Jong, K. P.; de Jongh, P. E. *Nat. Mater.* **2013**, *12*, 34−39.
(4) Cao, A.; Veser, G. *Nat. Mater.* **2010**, *9*, 75−81.
(5) Zhu, X.; Cho, H.; Pasupong, M.; Regalbuto, J. R. *ACS Catal.* **2013**, *3*, 625−630.
(6) Calderone, V. R.; Shiju, N. R.; Curulla-Ferré, D.; Chambrey, S.; Khodakov, A. Y.; Rose, A.; Thiessen, J.; Jess, A.; Rothenberg, G. *Angew. Chem., Int. Ed.* **2013**, *52*, 4397−4401.
(7) Rane, S.; Borg, Ø.; Rytter, E.; Holmen, A. *Appl. Catal., A* **2012**, *437−438*, 10−17.
(8) Girardon, J. S.; Quinet, E.; Gribovalconstant, A; Chernavskii, P.; Gengembre, L.; Khodakov, A. Y. *J. Catal.* **2007**, *248*, 143−157.
(9) Girardon, J. S.; Lermontov, A. S.; Gengembre, L.; Chernavskii, P. A. *J. Catal.* **2005**, *230*, 339−352.

(10) Bae, J. W.; Kim, S.-M.; Kang, S.-H.; Chary, K. V. R.; Lee, Y.-J.; Kim, H.-J.; Jun, K.-W. *J. Mol. Catal. A: Chem.* **2009**, *311*, 7−16.
(11) Kok, E.; Cant, N.; Trimm, D.; Scott, J. *Catal. Today* **2011**, *178*, 79−84.
(12) Rodríguez-González, V.; Marceau, E.; Beaunier, P.; Che, M.; Train, C. *J. Solid State Chem.* **2007**, *180*, 22−30.
(13) Marceau, E.; Löfberg, A.; Giraudon, J.-M.; Négrier, F.; Che, M.; Leclercq, L. *Appl. Catal., A* **2009**, *362*, 34−39.
(14) Zhang, L.; Dong, L.; Yu, W.; Liu, L.; Deng, Y.; Liu, B.; Wan, H.; Gao, F.; Sun, K.; Dong, L. *J. Colloid Interface Sci.* **2011**, *355*, 464−471.
(15) Marceau, E.; Che, M.; Čejka, J.; Zukal, A. *ChemCatChem.* **2010**, *2*, 413−422.
(16) Borg, Ø.; Dietzel, P. D. C.; Spjelkavik, A. I.; Tveten, E. Z.; Walmsley, J. C.; Diplas, S.; Eri, S.; Holmen, A.; Rytter, E. *J. Catal.* **2008**, *259*, 161−164.
(17) Hong, J.; Marceau, E.; Khodakov, A. Y.; Griboval-Constant, A.; La, C.; Briois, V.; Chernavskii, P. A. *Catal. Today* **2011**, *175*, 528−533.
(18) Dumond, F.; Marceau, E.; Che, M. *J. Phys. Chem. C* **2007**, *111*, 4780−4789.
(19) Qiu, S.; Zhang, X.; Liu, Q.; Wang, T.; Zhang, Q.; Ma, L. *Catal. Commun.* **2013**, *42*, 73−78.
(20) Sietsma, J. R. A.; Meeldijk, J. D.; den Breejen, J. P.; Versluijs-Helder, M.; van Dillen, J. A.; de Jongh, P. E.; de Jong, K. P. *Angew. Chem., Int. Ed.* **2007**, *46*, 4547−4549.
(21) Munnik, P.; Wolters, M.; Gabrielsson, A.; Pollington, S. D.; Headdock, G.; Bitter, J. H.; de Jongh, P. E.; de Jong, K. P. *J. Phys. Chem. C* **2011**, *115*, 14698−14706.
(22) Van de Loosdrecht, J.; Barradas, S.; Caricato, E. A.; Ngwenya, N. G.; Nkwanyana, P. S.; Rawat, M.; Sigwebela, B. H.; van Berge, P. J.; Visagie, J. L. *Top. Catal.* **2003**, *26*, 121−127.
(23) Wolters, M.; Munnik, P.; Bitter, J. H.; de Jongh, P. E.; de Jong, K. P. *J. Phys. Chem. C* **2011**, *115*, 3332−3339.
(24) Huang, C.; Bai, S.; Lv, J.; Li, Z. *Catal. Lett.* **2011**, *141*, 1391−1398.
(25) Boubekr, F.; Davidson, A.; Casale, S.; Massiani, P. *Microporous Mesoporous Mater.* **2011**, *141*, 157−166.
(26) Huang, X.; Dong, W.; Wang, G.; Yang, M.; Tan, L.; Feng, Y.; Zhang, X. *J. Colloid Interface Sci.* **2011**, *359*, 40−46.
(27) Imperor-Clerc, M.; Bazin, D.; Appay, M.; Beaunier, P.; Davidson, A. *Chem. Mater.* **2004**, *16*, 1813−1821.
(28) Hong, J.; Marceau, E.; Khodakov, A. Y.; Griboval-Constant, A.; La Fontaine, C.; Briois, V. *Chem.—Eur. J.* **2012**, 2802−2805.
(29) Neimark, A. V.; Kheifez, L. I.; Fenelonov, V. B. *Ind. Eng. Chem. Prod. Res. Dev.* **1981**, 439−450.
(30) Lekhal, A.; Glasser, B. J.; Khinast, J. G. *Chem. Eng. Sci.* **2001**, *56*, 4473−4487.
(31) Liu, X.; Khinast, J. G.; Glasser, B. J. *Chem. Eng. Sci.* **2012**, *79*, 187−199.
(32) Eggenhuisen, T. M.; Munnik, P.; Talsma, H.; de Jongh, P. E.; de Jong, K. P. *J. Catal.* **2013**, *297*, 306−313.
(33) Eggenhuisen, T. M.; Friedrich, H.; Nudelman, F.; Zečević, J.; Sommerdijk, N. A. J. M.; de Jongh, P. E.; de Jong, K. P. *Chem. Mater.* **2013**, *25*, 890−896.
(34) Munnik, P.; de Jongh, P. E.; de Jong, K. P. *J. Am. Chem. Soc.* **2014**, *136*, 7333−7340.
(35) Hao, X.; Spieker, W. A.; Regalbuto, J. R. *J. Colloid Interface Sci.* **2003**, *267*, 259−264.
(36) Wolters, M.; Andrade, I. C. A. C.; Munnik, P.; Bitter, J. H.; de Jongh, P. E.; de Jong, K. P. *Stud. Surf. Sci. Catal.* **2010**, *175*, 69−76.
(37) Becker, H.; Turek, T.; Güttel, R. *Catal. Today* **2013**, *215*, 8−12.
(38) Wolters, M.; Daly, H.; Goguet, A.; Meunier, F. C.; Hardacre, C.; Bitter, J. H.; de Jongh, P. E.; de Jong, K. P. *J. Phys. Chem. C* **2010**, *114*, 7839−7845.
(39) Sun, X.; Shi, Y.; Zhang, P.; Zheng, C.; Zheng, X.; Zhang, F.; Zhang, Y.; Guan, N.; Zhao, D.; Stucky, G. D. *J. Am. Chem. Soc.* **2011**, *133*, 14542−14545.
(40) Kletenik-Edelman, O.; Ploshnik, E.; Salant, a.; Shenhar, R.; Banin, U.; Rabani, E. *J. Phys. Chem. C* **2008**, *112*, 4498−5406.
(41) Kletenik-Edelman, O.; Sztrum-Vartash, C. G.; Rabani, E. *J. Mater. Chem.* **2009**, *19*, 2872−2876.
(42) Stannard, A. *J. Phys.: Condens. Matter* **2011**, *23*, 083001.
(43) Stannard, A.; Martin, C. P.; Pauliac-Vaujour, E.; Moriarty, P.; Thiele, U. *J. Phys. Chem. C* **2008**, *112*, 15195−15203.
(44) Vancea, I.; Thiele, U.; Pauliac-Vaujour, E.; Stannard, A.; Martin, C. P.; Blunt, M.; Moriarty, P. *Phys. Rev. E* **2008**, *78*, 1−15.
(45) Geus, J. W. In *Catalyst Preparation: Science and Engineering*; Regalbuto, J. R., Ed.; CRC Press: Boca Raton, FL, 2007; pp 341−372.
(46) Vakros, J.; Bourikas, K.; Perlepes, S.; Kordulis, C.; Lycourghiotis, A. *Langmuir* **2004**, *20*, 10542−10550.
(47) Ataloglou, T.; Fountzoula, C.; Bourikas, K.; Vakros, J.; Lycourghiotis, A.; Kordulis, C. *Appl. Catal., A* **2005**, *288*, 1−9.
(48) Van de Water, L. G. A.; Bezemer, G. L.; Bergwerff, J. A.; Versluijs-Helder, M.; Weckhuysen, B. M.; de Jong, K. P. *J. Catal.* **2006**, *242*, 287−298.
(49) Jacobs, G.; Ma, W.; Davis, B. H.; Cronauer, D. C.; Jeremy Kropf, A.; Marshall, C. L. *Catal. Lett.* **2010**, *140*, 106−115.
(50) Borg, Ø.; Walmsley, J. C.; Dehghan, R.; Tanem, B. S.; Blekkan, E. A.; Eri, S.; Rytter, E.; Holmen, A. *Catal. Lett.* **2008**, *126*, 224−230.
(51) Saib, A. M.; Moodley, D. J.; Ciobîc, I. M.; Hauman, M. M.; Sigwebela, B. H.; Weststrate, C. J.; Niemantsverdriet, J. W.; van de Loosdrecht, J. *Catal. Today* **2010**, *154*, 271−282.
(52) Van De Loosdrecht, J.; Datt, M.; Visagie, J. L. *Top. Catal.* **2013**, *57*, 430−436.
(53) Bezemer, G. L.; Bitter, J. H.; Kuipers, H. P. C. E.; Oosterbeek, H.; Holewijn, J. E.; Xu, X. D.; Kapteijn, F.; van Dillen, J. A.; de Jong, K. P. *J. Am. Chem. Soc.* **2006**, *128*, 3956−3964.
(54) Den Breejen, J. P.; Radstake, P. B.; Bezemer, G. L.; Bitter, J. H.; Frøseth, V.; Holmen, A.; de Jong, K. P. *J. Am. Chem. Soc.* **2009**, *131*, 7197−7203.
(55) Prieto, G.; Martínez, A.; Concepción, P.; Moreno-Tost, R. *J. Catal.* **2009**, *266*, 129−144.
(56) Borg, Ø.; Hammer, N.; Eri, S.; Lindvag, O. A.; Myrstad, R.; Blekkan, E. A.; Ronning, M.; Rytter, E.; Holmen, A. *Catal. Today* **2009**, *142*, 70−77.
(57) Saib, A. M.; Claeys, M.; van Steen, E. *Catal. Today* **2002**, *71*, 395−402.
(58) Prieto, G.; Martínez, A.; Murciano, R.; Arribas, M. A. *Appl. Catal., A* **2009**, *367*, 146−156.
(59) Iglesia, E. *Appl. Catal., A* **1997**, *161*, 59−78.